SYNTHESIS AND CHARACTERIZATION OF COMPOSITES BASED ON HYDROXYAPATITE NANOPARTICLES AND CHITOSAN EXTRACTED FROM SHELLS OF THE FRESHWATER CRAB *Potamon algeriense*

Mohammed Lakrat[1], Soufiane Fadlaoui[2*], Mohamed Aaddouz[1], Ouahid El Asri[3], Mohammed Melhaoui[2], El Miloud Mejdoubi[1]

[1] Laboratory of Mineral Solid and Analytical Chemistry (LMSAC), Department of Chemistry, Faculty of Sciences, Mohamed 1st University, Oujda, Morocco.

[2]Laboratory of Water, Environment, and Sustainable Development, Mohamed First University, Oujda, Morocco.

[3]Microbiology and Biotechnology Laboratory, Faculty of Sciences, Ibn Zohr University, Agadir, Morocco.

** e-mail: soufiane.fadlaoui@gmail.com*

Abstract

Nanocrystalline hydroxyapatite (n-HAp), which has low crystallinity, has attracted great attention due to its similarity to the inorganic part of human bone. Therefore, many studies have focused on creating new formulations combining n-HAp with some biopolymers, such as chitosan, in order to imitate biological bone tissue. The importance of chitosan and its derivatives in biomedical applications has grown significantly in the last three decades due to its biodegradability and renewable source. Besides, chitosan and its derivatives present excellent biocompatibility and biofunctionality, which make them promising materials in bone tissue engineering. In the present study, the chitosan was, first, extracted from the shell of the freshwater crab species Potamon algeriense following demineralization, deproteinization, decolouration (raw chitin) and deacetylation (chitosan) steps. Then, a novel composite based on n-HAp and extracted chitosan (CTS) with varying chitosan contents, from 5% to 20% (w/w), was synthesized and characterized for potential application in tissue regeneration. The obtained composites were characterized using X-ray diffraction, Fourier transform infrared spectroscopy and thermogravimetric analysis. The precipitated n-HAp/CTS nanocomposites similar to natural bone are promising composites for bone tissue engineering applications.

Keywords: *chitosan, nanocrystalline hydroxyapatite, nanocomposites, bone tissue engineering, freshwater crab, Potamon algeriense*

Received: 27.02.2020
Accepted: 04.05.2020

1. Introduction

Calcium phosphate hydroxyapatite ($Ca_{10}(PO_4)_6(OH)_2$) (HAp) represents approximately 70% of the human bone composition in a nanocrystalline form (n-Hap), with a size of 20–80 nm [1]. During the last decades, n-Hap has become an attractive material to be studied, especially in the field of biomaterials and bone tissue engineering, due to its excellent biocompatibility, bioactivity and osteoconductivity [2]. Furthermore, n-HAp has the ability to bond directly with neighbouring tissues when implanted, without any toxic or inflammatory effects [3].

To imitate natural bone, which mainly contains n-HAp and collagen, n-HAp has been widely used with many biopolymers such as polymethyl methacrylate, poly-L-lactide (PLA), poly(glycolic acid) and polysaccharides [4]. The low cytotoxicity and the good biocompatibility and resorbability of these biopolymers have attracted attention in the bone tissue engineering field.

Chitin is the most common polysaccharide in nature after cellulose. In the animal kingdom, it exists as a complex with proteins and minerals [5]. It is particularly present in marine invertebrates: it constitutes the shell of crustaceans and molluscs [6]. Chitin is also present in the exoskeleton of insects. In the plant kingdom, chitin is found in the lining of most fungi and some chlorophyceous algae [7]. Chitin is also present in some yeast and bacteria.

Chitosan (CTS), a deacetylated derivative of chitin, is a β-(1→4) linear copolymer of N-acetyl-D-glucosamine and D-glucosamine. It is more rarely found in nature: it is present only in the wall of a particular class of fungi and in a few insects. These two biopolymers are distinguished by the degree of acetylation (DA). In general, we refer to CTS when more than 50% of the glucosamine functions are deacetylated.

During the last three decades, chitin and its derivatives, mainly CTS, have attracted the interest of many researches for potential and applications [8]. In fact, chitin and CTS have many interesting physicochemical and biological properties (biocompatibility, bioactivity, nontoxicity and biodegradability) that have led to many potential applications [9]. CTS has attracted more interest than chitin due to the wide range of applications in different fields, e.g. cosmetics, agriculture, food industry, pharmacy, paper industry, paint, textile industries, wastewater treatment, wound healing and drug delivery systems [10]. Due to its biocompatibility with human tissues, CTS has demonstrated its high effectiveness for numerous medical applications especially in orthopaedics and dentistry [11]. Kim et al. [12] demonstrated the application of CTS and its derivatives in artificial organs such as the liver, nerves, bones, skin, cartilage, blood vessels, etc. While certain studies have used commercial CTS for the preparation of composites for bone tissue engineering, there have been some data on the exploitation of natural CTS for the same purposes [13]. The combination of natural CTS and n-HAp is reportedly a promising composite for many medical applications either in orthopaedics or dentistry [14].

The aim of this study was to valourize, for the first time, the CTS extracted from the shells of the freshwater crab *Potamon algeriense* from a previous work [15] by blending it with n-HAp using a co-precipitation method for potential medical applications. The generated composites were characterized using X-ray diffraction (XRD) and Fourier transform infrared spectroscopy (FTIR). Simultaneous thermogravimetric analysis (TGA) was utilized to evaluate the thermal stability of as-prepared composites.

2. Materials and Methods

2.1. Preparation of Chitin and CTS

For the preparation of chitin and CTS [15], specimens of the freshwater crab *P. algeriense* from Oued Zegzel (a mountain stream in northeast Morocco) were used

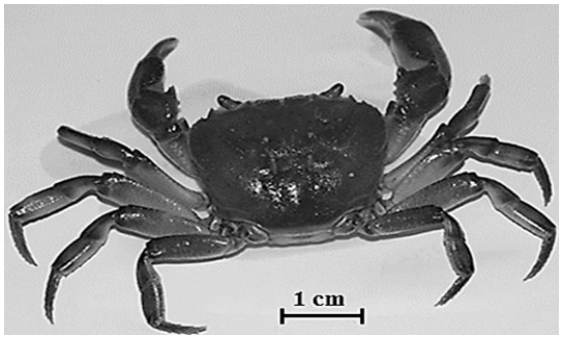

Figure 1. The freshwater crab *Potamon algeriense* [15].

(Fig. 1). Individuals were boiled for 15 min to remove them from their carapaces. The shells were scraped free of soft tissue, cleaned, rinsed and dried at 60°C for 24 h; ground with a Retsch mill (model Brinkmann Rmo) to obtain a coarse powder; and then passed through a 350-µm diameter sieve. CTS was prepared from the shells following the chemical protocol: demineralization, deproteinization, decolouration and deacetylation.

For the demineralization, the ground shells were then soaked in a 1 N HCl (ACS reagent, 37%, Sigma-Aldrich) solution for 6 h at room temperature to remove calcium salts with a solid/solvent ratio of 1:15 (w/v) [16]. The decalcified shell was collected on a Whatman paper filter in a Buchner funnel, washed with deionized water, dried and weighed.

Deproteinization was carried out using an autoclave (15 psi/121°C). The demineralized sample was treated with aqueous 3% sodium hydroxide (NaOH, Sigma-Aldrich S8045) solution for 20 min at 15 psi/121°C and a solid/solvent of ratio of 1:10 (w/v) [17]. The raw chitin was then washed, filtered, dried and weighed.

For decolouration, the raw chitin was further treated with a 0.32% sodium hypochlorite (NaClO, Sigma-Aldrich 425044) solution for 10 min with a solid/solvent ratio of 1:10 (w/v) [16]. Following decolouration, the sample was then washed, filtered, dried and weighed. For deacetylation, the decoloured raw chitin was treated at 15 psi/121°C with 50% NaOH for 30 min and a solid/solvent ratio of 1:15 (w/v) [18]. The resulting CTS was filtered, washed, dried and weighed.

2.2. n-Hap/CTS Composite Preparation

In order to prepare the n-Hap/CTS composites, different aqueous CTS solutions were prepared by dissolving the required amount of CTS in 4 wt% acetic acid (CH_3COOH, ACS Reagent Grade 320099) and stirring for 5 h. Then, the co-precipitation process [19] was adopted for the preparation of n-Hap/CTS nanocomposites with different CTS weight ratios (Table 1). The CTS solution was dispersed into a 0.02 M di-ammonium hydrogen phosphate solution [$(NH_4)_2HPO_4$, 98.7%, Fisher Chemical]. The mixed CTS/$(NH)_2HPO_4$ solution was then added drop-wise into the 0.03 M calcium nitrate [$(Ca(NO_3)_2 \cdot 4H_2O$, 99%, Sigma-Aldrich] solution while being agitated. The pH of the final solution was adjusted to 10 by adding an adequate amount of ammonium hydroxide solution (NH_4OH 35%, Fisher Chemical). The process is schematically represented in Fig. 2.

The resulting solution was kept in maturation for 24 h with gentle stirring. Finally, the precipitated n-HAp/CTS was filtered, washed with distilled water and dried at 80º C. The details for each composite are tabulated in Table 1.

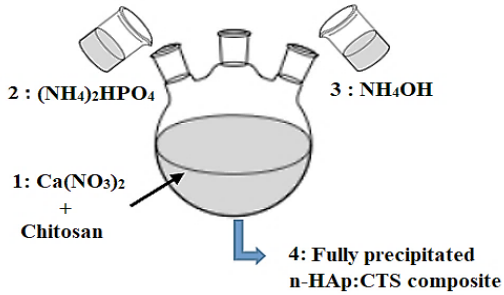

Figure 2. Schematic representation of the of nanocrystalline hydroxyapatite (n-Hap)/ chitosan (CTS) composite preparation.

Table 1. Composition of the prepared nanocrystalline hydroxyapatite (n-Hap)/extracted chitosan (CTS) composites

	n-Hap, wt%	**CTS, w%**
n-HAp/CTS 5	95	5
n-HAp/CTS 10	90	10
n-HAp/CTS 20	80	20

2.3. Characterization

2.3.1. FTIR analysis

FTIR was performed at room temperature in the range of 400–4000 cm^{-1} to identify the functional groups in the chitin as well as in n-HAp/CTS composites. The powders were mixed with potassium bromide (KBr), pressed into a pellet and analysed with a resolution of 2 cm^{-1}, with an accumulating of 32 scans, using a FTIR-8400S spectrometer (Shimadzu, Japan).

The degree of deacetylation (DD) of isolated CTS was estimated using FTIR spectroscopy from the absorption ratio A_{1560}/A_{1070} (equation 1) [20]:

$$DD\ (\%) = \frac{A1560}{A1070} \times 100, \quad (1)$$

where A_{1560} and A_{1070} are the intensity of the characteristic band located at 1560 and 1070 cm^{-1} respectively.

2.3.2. XRD analysis

For phase identification, the chitin and different composites were characterized using XRD. The diffraction patterns were acquired on a Shimadzu XRD-6000 using CuKα radiation (λ = 1.542 Å) at 35 kV and 10 mA. The composites were scanned with 2θ (where θ is the Bragg angle) varying from 10 to 70° with a step size of 0.02°.

2.3.3. TGA

TGA of the prepared composites was carried out in a nitrogen atmosphere using a Shimadzu DTG-60/60 machine. The measurements were recorded up 900°C at a heating rate of 10°C min^{-1}.

3. Results and Discussion

3.1. X-Ray Diffractogram of Extracted Chitin and Different Composites

Fig. 3 represents the XRD pattern of the extracted chitin. The crystalline components in the extracted sample revealed the characteristic chitin and collagen bands in the calcite planes. Thus, the XRD patterns reported that the biggest diffraction face intensity is located at 2Θ = 29.4, which corresponds to the rhombohedra calcite [21]. According to the literature, chitin has classic sharp peaks at 9 and 19.8°. The comparison of our XRD diffraction results with different types of calcite (012, 140, 110, 113, 202, 018, 116, 122 and 211) showed that it is similar to the strongest faces of calcite. Characteristic chitin peaks at 2Θ = 23, 37 and 57° [22] revealed that the chitin extracted from the *P. algeriense* has an alpha character [23].

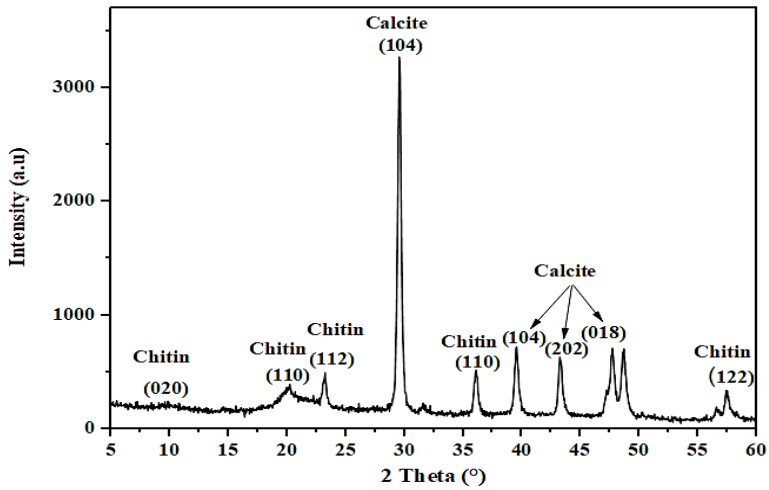

Figure 3. X-ray diffraction (XRD) analysis of chitin obtained from *Potamon algeriense*.

The XRD patterns of different n-Hap/CTS composites are given in Fig. 4. All composite patterns matched with the Joint Committee on Powder Diffraction Standards (JCPDS) file No. 09-432; they had a single phase of hydroxyapatite and no other calcium phosphate phases. Furthermore, the patterns showed that the XRD crystallinity of composites decreased with increasing chitin content, a finding that is consistent with previous investigations [24].

The crystallite sizes of n-HAp particles precipitated in the composites were determined by the Debye–Scherrer equation (Eq. 2) [25] using two XRD diffraction peaks (002 and 310) that give, respectively, the crystallite length and an average of their width/thickness:

$$D = \frac{0.9\lambda}{\beta \cos\theta}, \tag{2}$$

where D is the crystallite size in nm, λ is the radiation wavelength (0.154 nm), β represents the full width at half maximum of the peak and θ is the diffraction angle of the associated (hkl) plane.

All composites exhibited nanoparticle sizes at 5–7 nm in diameter by 9–12 nm in length (Table 2). These results confirmed the nanosize of the precipitated hydroxyapatite

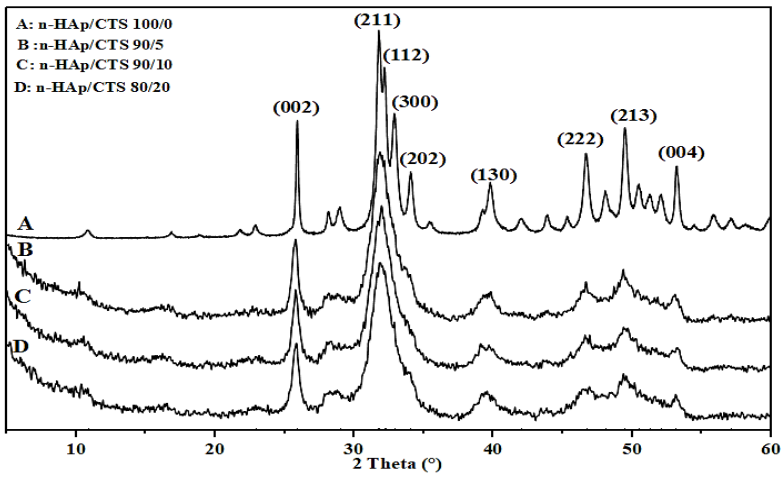

Figure 4. X-ray diffraction (XRD) patterns of (A) nanocrystalline hydroxyapatite (n-Hap) and (B–D) different n-Hap/chitosan (CTS) composites.

nanoparticles in the different composites. For biomedical applications, composites containing hydroxyapatite nanoparticles with low crystallinity are highly recommended because of their high *in vivo* resorbability rate [26]. The elaboration of extracted CTS and n-HAp using the co-precipitation method could be considered an effective way to produce nanocomposites for medical applications.

Table 2. Crystallite size of nanocrystalline hydroxyapatite (n-Hap) in the composites.

	Length (nm)	Width (nm)
n-HAp/CTS 95/5	9 ± 2	5.65 ± 1
n-HAp/CTS 90/10	10 ± 2	6.5 ± 1
n-HAp/CTS 80/20	12 ± 2	7 ± 1

Abbreviation: CTS, chitosan.

In addition, the n-Hap particles exhibited growth along the c axis, which in line with the anisotropic growth observed in biological hydroxyapatite particles [27] with 10–50 nm crystallite sizes [1]. Hence, the crystallite size of n-HAp increased with increase in the content of CTS in the nanocomposite. This increase of crystal size was attributed to n-HAp particle growth in the composite system by the CTS chain [28]. These results indicate that the precipitation of HAp particles in the composites was significantly influenced by the amount of CTS used.

3.2 FTIR analysis

The FTIR spectrum of CST (Fig. 5) revealed characteristic vibrational bands around 3437 cm^{-1}, which is attributed to the stretching vibration of $_{vs}$(N-H), while the band observed at 1651 cm^{-1} is attributed to $_{v}$(C=O) amide I carbonyl stretching. The peaks observed in the range of 1423 cm^{-1} correspond to the δ (C-H) symmetrical deformation and the bands located at 1074 cm^{-1} are related to $_{vs}$(C-O-C) stretching vibration [29]. The DD result of CST is approximately 83%, which indicates good solubility in water.

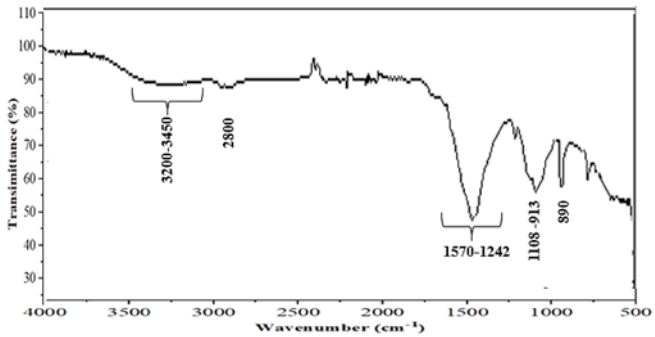

Figure 5. Fourier transform infrared spectra of the extracted chitosan.

The FTIR spectra of different composites are given in Fig. 6. The obtained spectra showed that all the major absorbance bands correspond to hydroxyapatite structure and their width increases significantly with increased CTS content. Furthermore, the absorption bands located at 950–1100 cm^{-1} and 550– 630 cm^{-1} are attributed to different modes of the PO_4^{3-} groups in the hydroxyapatite structure [30]surrounding tissues and implanted biomaterials always occur at their interfaces, the surface properties of potential implants appear to be of paramount importance for the clinical success. In view of the fact that a limited amount of materials appear to be tolerated by living organisms, a special discipline called surface engineering was developed to initiate the desirable changes to the exterior properties of various materials but still maintaining their useful bulk performances. In 1975, this approach resulted in the introduction of a special class of artificial bone grafts, composed of various mechanically stable (consequently, suitable for load bearing applications. The broadening of the band located at 1050 cm^{-1} revealed the presence of polymer and its interaction with the phosphate groups (PO^{3-}).

The band at 1643 cm^{-1} corresponds to the superposition of CTS amide I and amide II groups and the hydroxyapatite OH^- group [31]. Furthermore, the small peaks at 1420 cm^{-1}

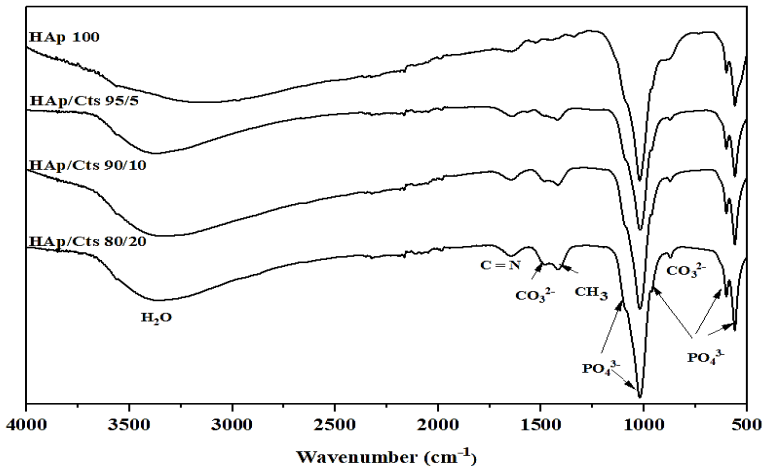

Figure 6. Fourier transform infrared spectra of nanocrystalline hydroxyapatite (n-Hap) and n-Hap/chitosan (CTS) composite.

DOI: 10.15259/PCACD.25.010

are assigned to the CH_3 symmetrical deformation mode [32]. There were also carbonate bands (CO_3^{2-}) around at 1448 and 872 cm^{-1}. The bands around 3600–3700 cm^{-1} and 2800–2950 cm^{-1} are assigned to the hydroxyl groups present in CTS [33]. Comparing the FTIR spectra of pure hydroxyapatite and CTS/n-HAp composites suggests that characteristic bands of both phases n-HAp and CTS are present in the differences nanocomposites.

3.3. Thermal analysis

A more direct test of the constituent of n-Hap/CTS composites was provided by TGA. The curves of pure n-Hap, extracted CTS and the different precipitated composites are given in Fig. 7, which plots weight loss versus temperature. For pure n-Hap, there was no notable weight loss. However, the thermal behaviour of different composites comprised three steps, similar to the extracted CTS. The first stage in the range of 78–180°C is attributed to the evaporation of absorbed water. The second stage between 180 and 300°C is assigned to the beginning of the thermal decomposition of CTS chains. When the temperature increased from 300 to 550°C, the mass loss was higher due to the continued decomposition of CTS. Above 550°C, only hydroxyapatite remained, which explains the unchanged weight up to 900°C [34]. Therefore, the presence of n-HAp in the composites enhanced the thermal stability. Moreover, from the TGA curves, it can be concluded that the greater the CTS content, the greater the weight loss. These results confirm the presence of CTS and n-HAp in the precipitated composites.

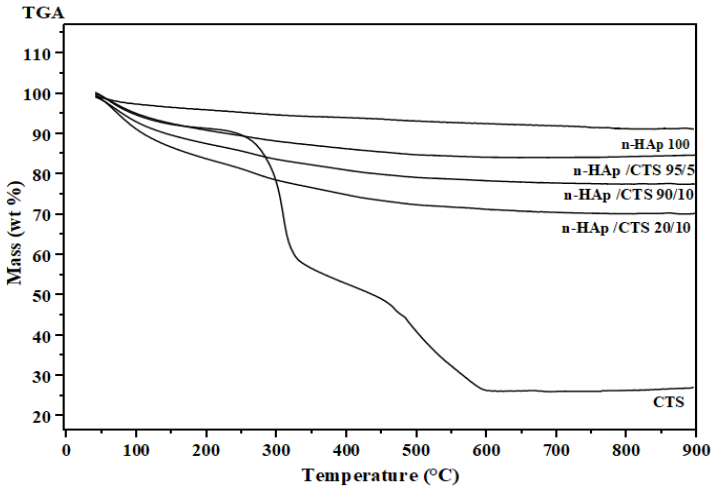

Figure 7. Thermogravimetric analysis of nanocrystalline hydroxyapatite (n-Hap)

4. Conclusion

n-Hap/CTS composites with various CTS ratios were successfully obtained using the co-precipitation method. XRD patterns of different n-HAp/CTS composites showed that it has a single phase of hydroxyapatite with low crystallinity and nanosized particles. FTIR spectra confirmed the presence of HAp and CTS. TGA of the prepared composite showed that all composites presented weight loss associated with the evaporation of adsorbed water and the thermal degradation of CTS. Moreover, from the TGA curves, it can be concluded that the greater the CTS content, the greater the weight loss. The above results

suggest that the nanocomposites with a structure and nanosize similar to biological apatite might be suitable for biomedical applications.

5. References

[1] Cunniffe GM, O'Brien FJ, Partap S, Levingstone TJ, Stanton KT, Dickson GR; (2010) The synthesis and characterization of nanophase hydroxyapatite using a novel dispersant-aided precipitation method, J. Biomed. Mater Res – Part A. 95 1142–1149. https://doi.org/10.1002/jbm.a.32931.

[2] Dorozhkin SV; (2010) Nanosized and nanocrystalline calcium orthophosphates, Acta Biomater. 6 715–734. https://doi.org/10.1016/J.ACTBIO.2009.10.031.

[3] Kantharia N, Naik S, Apte S, Kheur M, Kheur S, Kale B; (2014) Nano-hydroxyapatite and its contemporary applications. J Dent Res Sci Dev. 1 15. https://doi.org/10.4103/2348-3407.126135.

[4] Wei G, Ma PX; (2004) Structure and properties of nano-hydroxyapatite/polymer composite scaffolds for bone tissue engineering. Biomaterials. 25 4749–4757. https://doi.org/10.1016/j.biomaterials.2003.12.005.

[5] Sudarshan NR, Hoover DG, Knorr D; (1992) Antibacterial Action of Chitosan. Food Biotechnol. 6 257–272. https://doi.org/10.1080/08905439209549838.

[6] Rashidova SS, Milusheva RY, Voropaeva NL, Pulatova SR, Nikonovich GV, Ruban IN; (2004) Isolation of chitin from a variety of raw materials, modification of the material, and interaction its derivatives with metal ions. Chromatographia. 59 783–786. https://doi.org/10.1365/s10337-004-0290-0.

[7] Ravi Kumar MNV; (2000) A review of chitin and chitosan applications. React Funct Polym. 46 1–27. https://doi.org/10.1016/S1381-5148(00)00038-9.

[8] Wysokowski M, Szalaty TJ, Jesionowski T, Motylenko M, Rafaja D, Koltsov I, Stöcker H, Bazhenov VV, Ehrlich H, Stelling AL, Beyer J, Heitmann J, Petovic S, Đurović M; (2017) Extreme biomimetic approach for synthesis of nanocrystalline chitin-(Ti,Zr)O2 multiphase composites. Mater Chem Phys. 188 115–124. https://doi.org/10.1016/j.matchemphys.2016.12.038.

[9] Wang W, Cao N, Dong J, Boukherroub R, Liu W, Li Y, Cong H; (2019) Chitosan/hydroxyapatite modified carbon/carbon composites: synthesis, characterization and: in vitro biocompatibility evaluation. RSC Adv. 9 23362–23372. https://doi.org/10.1039/c8ra10396h.

[10] Sekiguchi S, Miura Y, Kaneko H, Nishimura SI, Nishi N, Iwase M, Tokura S; (1994) Molecular Weight Dependency of Antimicrobial Activity by Chitosan Oligomers. Food Hydrocoll. Springer US,: pp. 71–76. https://doi.org/10.1007/978-1-4615-2486-1_6.

[11] Zhao D, Yu S, Sun B, Gao S, Guo S, Zhao K; (2018) Biomedical applications of chitosan and its derivative nanoparticles, Polymers (Basel). https://doi.org/10.3390/polym10040462.

[12] Kim IY, Seo SJ, Moon HS, Yoo MK, Park IY, Kim BC, Cho CS; (2008) Chitosan and its derivatives for tissue engineering applications. Biotechnol Adv. 26 1–21. https://doi.org/10.1016/j.biotechadv.2007.07.009.

[13] Pighinelli L, Kucharska M; (2013) Chitosan-hydroxyapatite composites. Carbohydr Polym. 256–262. https://doi.org/10.1016/j.carbpol.2012.06.004.

[14] Boudemagh D, Venturini P, Fleutot S, Cleymand F; (2019) Elaboration of hydroxyapatite nanoparticles and chitosan/hydroxyapatite composites: a present status. Polym Bull. 76 2621–2653. https://doi.org/10.1007/s00289-018-2483-y.

[15] Fadlaoui S, El Asri O, Mohammed L, Sihame A, Omari A, Melhaoui M; (2019) Isolation and characterization of chitin from shells of the freshwater crab potamon

algeriense. Prog Chem Appl Chitin Its Deriv. 24 23–35. https://doi.org/10.15259/PCACD.24.002.

[16] No HK, Lee MY; (1995) Isolation of chitin from crab shell waste. J Kor Soc Food Nutri (Korea Republic).

[17] Cho HR, Chang DS, Lee WD, Jeong ET, Lee EW; (1998) Utilization of chitosan hydrolysate as a natural food preservative for fish meat paste products. Kor J Food Sci Tech. 30(4), 817–822.

[18] No HK, Lee KS, Meyers SP; (2000) Correlation between physicochemical characteristics and binding capacities of chitosan products. J Food Sci. 65 1134-1137. https://doi.org/10.1111/j.1365-2621.2000.tb10252.x.

[19] Mondal S, Pal U, Dey A; (2016) Natural origin hydroxyapatite scaffold as potential bone tissue engineering substitute. Ceram Int. 42 18338–18346. https://doi.org/10.1016/J.CERAMINT.2016.08.165.

[20] Duarte ML, Ferreira MC, Marvão MR, Rocha J; (2002) An optimised method to determine the degree of acetylation of chitin and chitosan by FTIR spectroscopy, Int. J. Biol. Macromol. https://doi.org/10.1016/S0141-8130(02)00039-9.

[21] Rahman MA, Halfar J; (2014) First evidence of chitin in calcified coralline algae: New insights into the calcification process of Clathromorphum compactum, Sci. Rep. 1–11. https://doi.org/10.1038/srep06162.

[22] Erdogan S, Kaya M, Akata I; (2017) Chitin extraction and chitosan production from cell wall of two mushroom species (Lactarius vellereus and Phyllophora ribis), in: AIP Conf. Proc., American Institute of Physics Inc. https://doi.org/10.1063/1.4975427.

[23] Kaya M, Sargin I, Tozak KO, Baran T, Erdogan S, Sezen G; (2013) Chitin extraction and characterization from Daphnia magna resting eggs, Int. J. Biol. Macromol. https://doi.org/10.1016/j.ijbiomac.2013.08.016.

[24] Dwiasih P, Hidayat N, Kurniawan R; (2019) Sonochemical Synthesis of Nano-Hydroxyapatite/Chitosan Biomaterial Composite from Shellfish and Their Characterizations, IOP Conf. Ser. Mater. Sci. Eng. https://doi.org/10.1088/1757-899X/515/1/012050.

[25] Scherrer P; (1918) Bestimmung der Größe und der inneren Struktur von Kolloidteilchen mittels Röntgenstrahlen, Nachrichten von Der Gesellschaft Der Wissenschaften Zu Göttingen, Math. Klasse. 98–100. https://eudml.org/doc/59018 (accessed October 13, 2018).

[26] Ebrahimpour A, Johnsson M, Richardson CF, Nancollas GH; (1993) The characterization of hydroxyapatite preparations, J. Colloid Interface Sci. https://doi.org/10.1006/jcis.1993.1307.

[27] Rey C, Shimizu M, Collins B, Glimcher MJ; (1990) Resolution-enhanced Fourier transform infrared spectroscopy study of the environment of phosphate ions in the early deposits of a solid phase of calcium-phosphate in bone and enamel, and their evolution with age. I: Investigations in the upsilon 4 PO4 domain. Calcif Tissue Int. 46 384–94. http://www.ncbi.nlm.nih.gov/pubmed/2364326 (accessed October 2, 2018).

[28] Kong L, Gao Y, Cao W, Gong Y, Zhao N, Zhang X; (2005) Preparation and characterization of nano-hydroxyapatite/chitosan composite scaffolds. J Biomed Mater Res - Part A. 75 275–282. https://doi.org/10.1002/jbm.a.30414.

[29] Manjubala I, Scheler S, Bössert J, Jandt KD; (2006) Mineralisation of chitosan scaffolds with nano-apatite formation by double diffusion technique, Acta Biomater. https://doi.org/10.1016/j.actbio.2005.09.007.

[30] Dorozhkin SV; (2015) Calcium orthophosphate deposits: Preparation, properties and biomedical applications. Mater Sci Eng C Mater Biol Appl. 55 272–326. https://doi.org/10.1016/j.msec.2015.05.033.

[31] Danilchenko SN; (2009) Chitosan–hydroxyapatite composite biomaterials made by a one step co-precipitation method: preparation, characterization and in vivo tests. J Biol Phys Chem. 9 119–126. https://doi.org/10.4024/22da09a.jbpc.09.03.
[32] Thein-Han WW, Misra RDK; (2009) Biomimetic chitosan-nanohydroxyapatite composite scaffolds for bone tissue engineering. Acta Biomater. 5 1182–1197. https://doi.org/10.1016/j.actbio.2008.11.025.
[33] Boulila S; (2016) Comportement de verres composites poreux : assimilation osseuse, explorations physiologiques et physico-chimiques, Http://Www.Theses.Fr. http://www.theses.fr/2016REN1S105 (accessed February 5, 2019).
[34] Chen J, Wang Z, Wen Z, Yang S, Wang J, Zhang Q; (2015) Controllable self-assembly of mesoporous hydroxyapatite. Colloids Surfaces B Biointerfaces. 127 47–53. https://doi.org/10.1016/j.colsurfb.2014.12.055.